Published in Solar Energy Materials and Solar Cells (2012), DOI 10.1016/j.solmat.2012.09.029

Fire-Through Contacts – A New Approach to Contact the Rear Side of Passivated Silicon Solar Cells

Benjamin Thaidigsmann*, Christopher Kick, Andreas Drews, Florian Clement, Andreas Wolf, Daniel Biro

Fraunhofer Institute for Solar Energy Systems ISE, Heidenhofstr. 2, D-79110 Freiburg, Germany

* Phone: +49-761-4588-5045, E-Mail: benjamin.thaidigsmann@ise.fraunhofer.de

Abstract

In this work, we present a novel fire-through contact (FTC) approach for the formation of local rear contacts for rear surface passivated silicon solar cells. The FTC approach aims at an easy integration of rear surface passivation into typical production lines. Besides rear surface passivation, no new technology is required as FTC only relies on common printing equipment. In this work, different FTC contact geometries and printing approaches are investigated using lifetime and resistance measurements. A PC1D model is implemented to allow for a comparison of different FTC configurations on cell level. Finally, the integration of the FTC approach into metal wrap through solar cells is presented.

Keywords: FTC, PERC, LFC, passivation, local contact, screen printing

1. Introduction

Along with the strongly increasing interest in solar cells with passivated rear surface, industrially feasible rear contacting methods gain importance. Usually, the fabrication of PERC-type cells (passivated emitter and rear cell, [1]) requires laser processing or other structuring process steps for the creation of local rear contacts. Currently, laser processing is the most dominant approach for industrial application, either applied before metallisation [2-4] (i-PERC) or after contact firing [5, 6] (laser fired contacts, LFC).

In this paper we present an easily scalable technology for contacting the rear side of PERC-type cells using solely printing technology. Analogous to the contact formation on the front side [7], local penetration of the dielectric layer during contact firing is the key aspect of this approach. For this purpose, a fire-through paste is printed locally on the top of the rear dielectric layer with a defined geometry. In a second step, a non-fire-through aluminium paste is printed on top, thus interconnecting the previously applied fire-through areas. Subsequently a high temperature process realises the contact formation.

With this novel FTC approach, one additional screen printing step substitutes local laser contact formation. This is beneficial for retrofitting of existing industrial Al-BSF-based production lines, as the printing based FTC method depends on a smaller number of technologies and does not require laser expertise. Compared to previous fire-through approaches [8], an additional benefit of the FTC technology is the decoupling of contact formation and lateral conductivity, thus providing the possibility to manipulate the paste for local BSF formation or the contact geometry without affecting the properties of the overlying Al layer. Furthermore, the rear contact is established during the common contact firing process, thus – in contrast to previous approaches [9] – no high temperature process is necessary after application of the fire-through paste.

2. Experimental

2.1 Approach

The FTC approach is applicable to solar cell structures that comprise a rear surface passivation and a large-area p-type rear contact. For the deposition of the FTC structure as well as the overlying large-area metallisation, various technologies may be utilised. This work focuses on stencil and screen printing of the fire-through paste and screen printed large-area Al layers. Figure 1 shows the intended process sequence for the FTC approach integrated into a typical PERC process sequence.

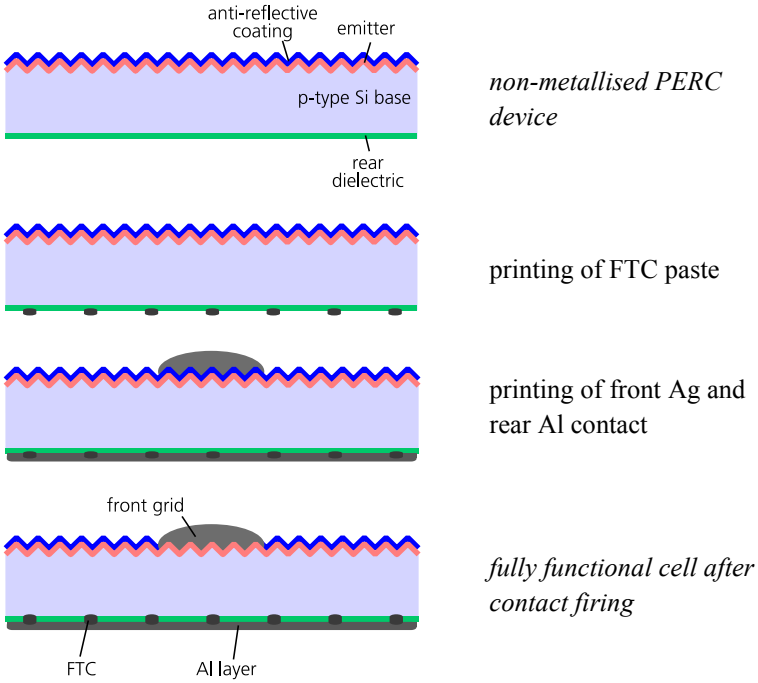

Figure 1: Process sequence for the fabrication of PERC devices with fire-through contacts (FTC).

The following sections present a detailed investigation of fire-through structures regarding contact resistance and recombination using special test structures.

2.2 Sample preparation

To investigate the relevant properties of the fire-through contacts – contact resistance and the influence of the fire-through process on the passivation quality – both resistance and carrier lifetime test structures (see Figure 2 and Figure 3) are fabricated from monocrystalline p-type silicon wafers with a thickness of 200 µm and an edge length of 125 mm. The resistance samples are made of float-zone silicon (FZ-Si) with a base resistivity of $\rho = 1$ Ωcm passivated by a stack of 100 nm thermally grown SiO_2 and 100 nm PECVD SiN_x on the rear side. The lifetime samples are made of Czochralski-grown silicon (Cz-Si) with a base resistivity of $\rho \approx 6$ Ωcm and the same SiO_2/SiN_x passivation layer stack on both sides.

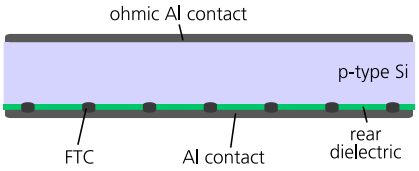

Figure 2: Resistance test structure for FTC resistance measurements.

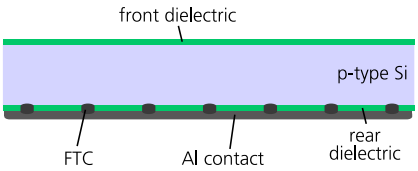

Figure 3: Carrier lifetime test structure used for evaluation of the recombination rate at the fire-through contacts.

A fire-through Al paste is printed on the rear side of the samples with the test layout depicted in Figure 4 using both stencil and screen printing. The design of this test structure with nine separated areas enables an investigation of various contact geometries on a single wafer. Afterwards, a full area non-fire-through aluminium layer is printed on top. After contact firing in an industrial belt furnace, the resistance samples are equipped with an ohmic full-area PVD-Al contact on the front side whereas the lifetime samples are treated with HCl/H_2O_2 in order to fully remove the rear Al structure and thus enable a QSSPC [10] measurement.

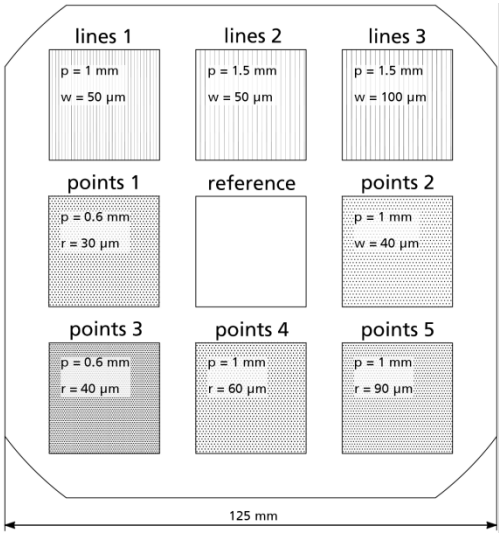

Figure 4: Test structure with different contact geometries (p: pitch, w: width, r: radius).

3. Results and discussion

3.1 Printing of fire-through structures

The desired fire-through areas only cover a small area fraction of the solar cell's rear side, thus especially stencil printing is a highly suitable technology for fast creation of well-defined FTC structures. The test layout depicted in Figure 4 is printed with a nickel stencil as well as a reference screen printing process. The individual contact geometries evaluated with the test structure represent different pre-optimised point- and line-shaped structures with feature sizes in the range of typical LFC and i-PERC contacts. Figure 5 displays an SEM cross section micrograph of dots printed with a stencil showing a high aspect ratio and sharp edges.

Printablility tests for the evaluation of a suitable fire-through paste were carried out. Figure 6 shows the average height profile of FTC line structures measured using confocal microscopy for four different pastes. Paste 1 is a special fire-through aluminium paste and shows the highest aspect ratio and the narrowest line width and is therefore selected as the most suitable FTC paste. This paste also showed up to 100 times lower contact resistance values in pretests (with typical solar cell contact firing temperatures) compared to the pastes 2-4. Thus, only paste 1 is used for the investigations described in the following sections.

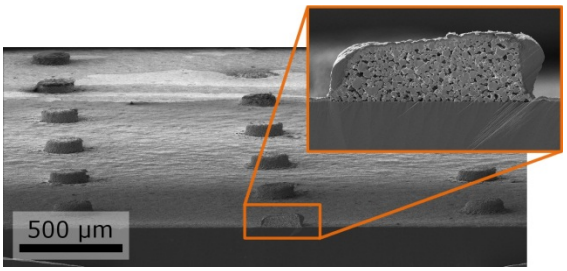

Figure 5: SEM micrograph of a stencil printed FTC Al dot after firing (structure "points 4"). The dots are covered by evaporated Al.

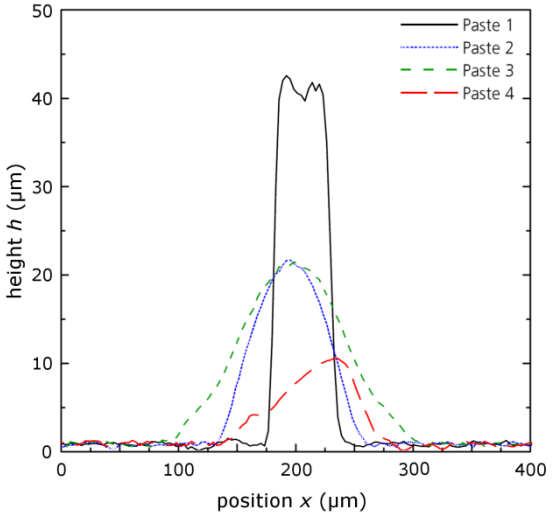

Figure 6: Height profile of stencil printed FTC line structures measured after firing (structure "lines 1", stencil thickness is 60 µm).

3.2 Electrical properties

Both low recombination and low contact resistance are important properties for local rear contacts. To allow for a comparison of different point- and line-shaped FTC structures, effective surface recombination velocity $S_{\text{eff,rear}}$ and total resistance R_{total} of the lifetime and the resistance samples are measured respectively.

As the lifetime samples are asymmetrical (see Figure 3), the effective rear surface recombination velocity

$$S_{\text{eff,rear}} = \frac{\tan(W\gamma_1)\ D^2\gamma_1^2 - S_{\text{front}} D\gamma_1}{\tan(W\gamma_1)\ S_{\text{front}} + D\gamma_1}$$

(W: wafer thickness, D: diffusion constant) is calculated using the effective lifetime τ_{eff} measured after wet chemical removal of the rear Al layer and the front surface recombination velocity S_{front} = 60.3 cm/s extracted from non-metallised, symmetrically passivated lifetime samples [11]. The parameter

$$\gamma_1 = \sqrt{\frac{\frac{1}{\tau_{\text{eff}}} - \frac{1}{\tau_{\text{b}}}}{D}}$$

is calculated assuming intrinsic carrier lifetime τ_b in the bulk [12].

Figure 7 shows $S_{\text{eff,rear}}$ for the different investigated contact geometries. Due to inhomogeneities in surface passivation quality the values show rather strong deviations. Nevertheless, the data allows for a general comparison of the different geometries and printing approaches. As expected, $S_{\text{eff,rear}}$ increases with increasing FTC area fraction. Stencil printing results in slightly increased recombination at point-shaped contacts which might originate from an increased amount of deposited paste and thus a higher fraction of actual contact area (see section 3.4).

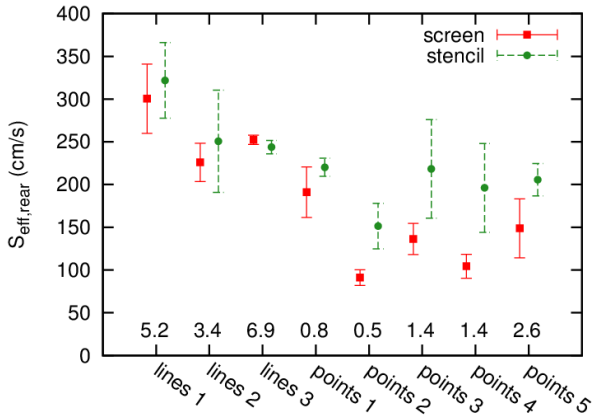

Figure 7: Effective rear surface recombination velocity $S_{\text{eff,rear}}$ and standard deviation extracted from a measurement after wet chemical removal of the rear Al layer. The samples are made from ~200 µm thick Cz-Si ($\rho \approx 6$ Ωcm) with SiO_2/SiN_x surface passivation. "screen" indicates screen printing, "stencil" indicates printing with a 30 µm thick Ni stencil. The desired area fraction of each FTC structure is given in the bottom line (in %). Each point represents 2 samples.

To get a comprehensive picture of the local contacts, the resistance has to be taken into account. The total measured resistance of the resistance samples is shown in Figure 8. All resistance samples are made from FZ-Si with a base resistivity of ρ = 1 Ωcm, allowing for a direct comparison of the tested contact geometries. The values directly correspond to the expected series resistance contribution of the rear contact in the finished device including the p-type base. Due to the small size of the actual contacts (see Figure 11) spreading resistance is assumed to dominate the total resistance resulting in a linear dependence of the series resistance upon base resistivity. Stencil printing yields the lowest resistance values almost for every structure. This is attributed to an increased amount of deposited paste and the well-defined shape of the printed structures. For both printing methods, the resistance decreases with increasing area coverage. Reference measurements reveal an average resistance of ~1000 Ωcm^2 for samples without fire-through structures confirming the non-fire-through properties of the full area Al layer.

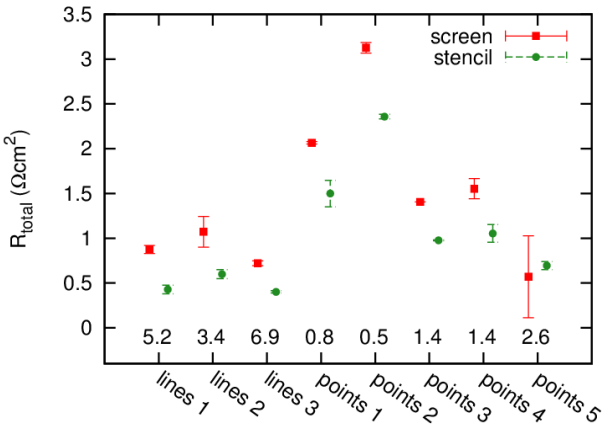

Figure 8: Total area-weighted resistance R_{total} and corresponding standard deviation of the resistance samples. The samples are made from 180 µm thick FZ-Si (ρ = 1 Ωcm). The desired area fraction of each FTC structure is given in the bottom line (in %). Each point represents 2 samples

The previously presented data alone does not suffice for an identification of the optimum contact geometry and printing method. The impact of both properties – series resistance contribution and effective surface recombination velocity – on conversion efficiency has to be taken into account. Thus, a simulation of solar cells with different rear contact properties is carried out in the next section.

3.3 Modelling of FTC-based solar cells

A PC1D model [13] of a PERC-type solar cell is implemented to allow for a rating of the investigated FTC configurations. The following parameters are used for the simulation:

- cell thickness: 150 µm
- base resistivity: 1.5 Ωcm
- effective bulk lifetime: 60 µs
- emitter sheet resistance: 75 Ω/sq (typical industrial doping profile)
- series resistance of front contact: 0.5 Ωcm^2.

The contour plot background colour in Figure 9 presents the simulated efficiencies for different rear surface recombination velocities S_{eff} and rear series resistances $R_{S,rear}$ and therefore allows for a rating of the corresponding average values determined for the different FTC configurations (lines 1 to 3 and points 1 to 5). The reference data for LFC are typical values for screen printed metallisation and SiO_2 based passivation [14] and a pitch of 500 µm. Due to the fact that the lifetime samples used for S_{eff} extraction have a resistivity of ~6 Ωcm, all S_{eff} values shown in the graph are scaled by a factor of 2 to get an estimation of the corresponding value for a PERC device with a typical base resistivity of 1.5 Ωcm [15]. Analogous, all resistance values R_{total} from the previous section are scaled by a factor of 1.5 to account for the resistivity of ρ = 1 Ωcm of the FZ-Si resistance samples assuming linear dependence of both spreading resistance and contact resistance.

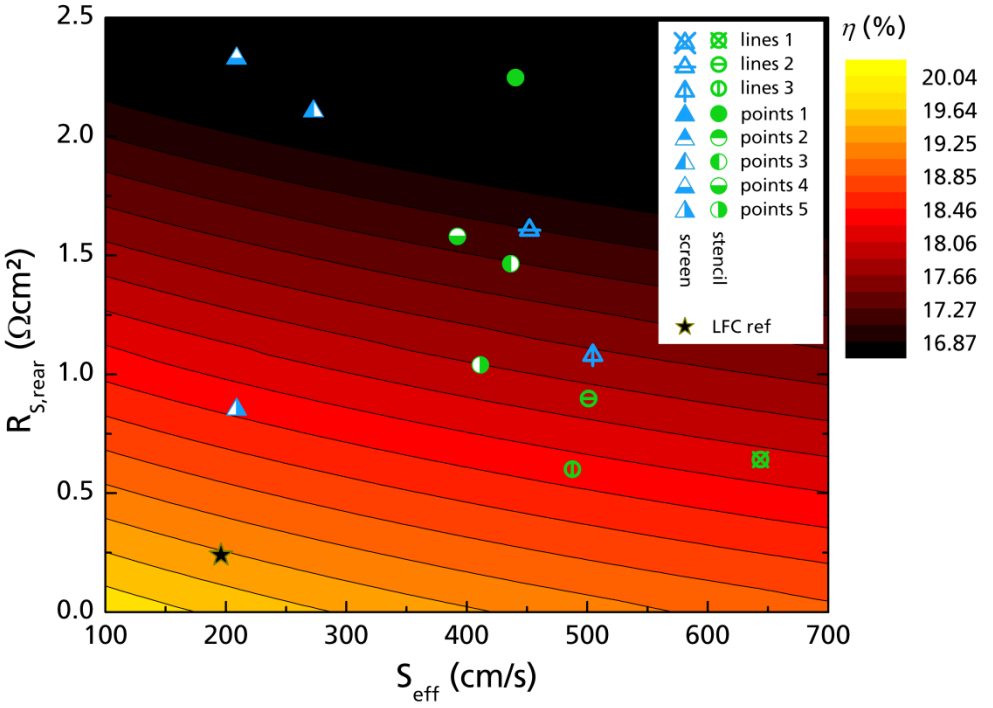

Figure 9: Average rear series resistance contribution $R_{S,rear}$ (including base) plotted against average effective rear surface recombination velocity S_{eff} for the investigated FTC configurations and corresponding efficiencies calculated with a PC1D model. Both $R_{S,rear}$ and S_{eff} values are scaled to account for a typical base resistivity of ρ = 1.5 Ωcm.

Obviously, highest efficiencies require low rear contact resistance and low surface recombination velocity. The most appropriate FTC configurations identified in the experiment are *points 5, screen-printed* and *lines 3, stencil-printed*. As the series resistance of the screen-printed structure *points 5* is surprisingly low and the standard deviation high (see Figure 8), the data of this structure is considered as being an outlier. Thus, the stencil printed structure *lines 3* is identified as being most appropriate. Compared to the LFC reference values, the FTC samples show reasonably low S_{eff} values but rather high resistance. This is assigned to non-optimal penetration of the rear surface passivation by the fire-through pastes (see next section). The fabrication of suitable pastes is still in an early stage of development and therefore strong improvements of the achievable efficiencies are expected after future optimisations of the paste composition.

3.4 Microstructure analysis of the local contacts

A microstructure analysis is carried out to improve the understanding of the contact formation and to further investigate the penetration of the dielectric by the fire-through paste. The SEM micrograph shown in Figure 10 confirms the successful penetration of the rear dielectric and the resulting local alloying of Al into Si. Nevertheless, the contacted areas are smaller than expected. Optical micrographs recorded after wet chemical removal of the rear aluminium (see Figure 11) reveal significant differences between the actual contact area and the area covered by FTC paste for both lines and points. This explains the rather high total resistance measured at the resistance samples (see previous section). Thus, further investigation of both dielectric layer properties and FTC paste composition seems necessary.

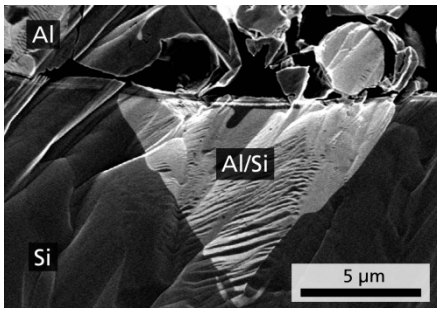

Figure 10: SEM micrograph of an FTC cross section. The Al/Si eutectic penetrates the p-type Si bulk in a pyramidal shape.

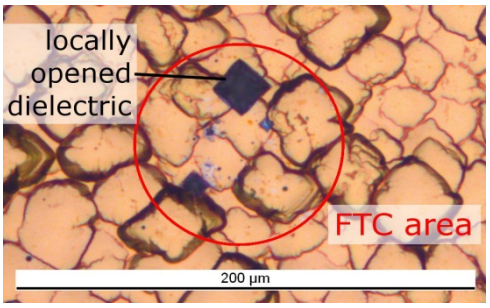

Figure 11: Exemplary micrograph of an FTC after removal of the Al layer. The actual contact area (dark squares) is much smaller than the area covered by the FTC paste (red circle).

3.5 Solar cell results

A preliminary solar cell batch is fabricated to evaluate the potential of the FTC approach. Bearing in mind that the achievable efficiency is limited by a rather high contact resistance of the currently used FTC paste composition, this first cell batch is thought of as a first proof of concept.

Small area metal wrap through passivated emitter and rear cells (MWT-PERC) are fabricated from FZ-Si (ρ = 0.5 Ωcm) similar to cells presented in earlier publications [16]. The thermal SiO_2/SiN_x rear surface passivation equals the one used for the lifetime and resistance samples presented in the previous sections. A small amount of cells features screen printed FTC rear contacts (similar to "points 5" as described above), reference cells with both LFC rear contacts and full-area Al back surface field (BSF) are processed in parallel.

The current-voltage characteristics shown in Table 1 are peak values achieved for each rear contacting method. Since the number of equally processed cells within each group is rather small, no median values are specified. As expected, an increased series resistance (corresponding to increased *pFF* - *FF*) limits the fill factor *FF* and thus the efficiency η of the FTC device, showing that the contact formation between the rear Al layer and the Si material needs to be improved. On the other hand, both open circuit voltage V_{OC} and short circuit current density j_{SC} of the FTC device exceed the values of the BSF reference cell and are close to the values of the LFC approach confirming the potential of the FTC approach. Note that the properties of the devices differ from the parameters used for the simulation in section 3.3, thus a direct comparison is not possible.

Table 1: Current voltage characteristics of MWT solar cells with fully screen printed metallisation fabricated from FZ-Si (ρ = 0.5 Ωcm) for FTC, LFC and BSF rear contact approach measured with an industrial cell tester. A reference cell measured at Fraunhofer ISE CalLab ensures accurate calibration of the measurement. Cell dimensions are 26.5 mm x 26.5 mm x 220 µm. All cells feature p- and n-type solder pads at the rear.

rear contact	η (%)	j_{SC} (mA/cm^2)	V_{OC} (mV)	*FF* (%)	*pFF* - *FF* (%)
FTC	18.3	38.7	640	73.8	6.2
LFC	20.0	39.3	645	79.0	3.4
BSF	18.7	37.8	629	78.2	1.9

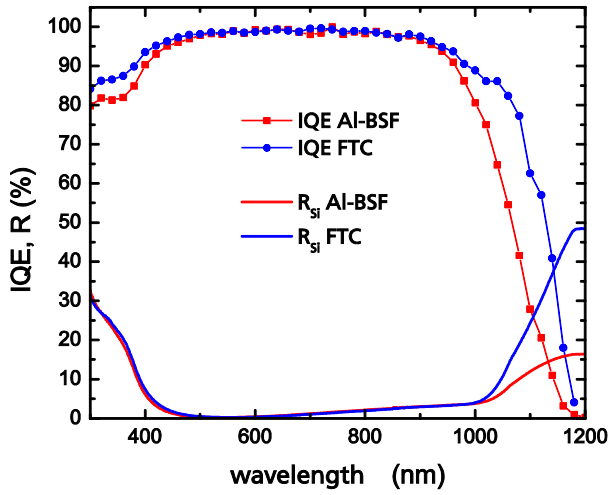

Figure 12: Internal quantum efficiency and reflectance data of MWT solar cells with full area Al back surface field (Al-BSF) and local fire-through contacts (FTC).

Figure 12 shows the internal quantum efficiency and reflectance for a cell with an FTC rear contact structure in comparison to a full area Al back surface field (Al-BSF). The data clearly confirms the improved rear surface passivation and light trapping of the FTC device.

4. Conclusion and outlook

A novel rear contacting method based solely on printing technology is introduced. This so called fire-through contact (FTC) approach is regarded as an ideal solution for retrofitting of already existing production lines to implement local rear contacting of surface passivated solar cells as screen printing is known as robust technology being widely used in solar cell manufacturing. Besides the creation of the surface passivation layer, no additional technology is required.

PC1D modelling of PERC-type solar cells with varying S_{eff} and $R_{S,rear}$ is used to rate various FTC configurations. Screen printed dots are integrated into a small area FZ-Si MWT-PERC device. The measured V_{OC} of 640 mV and j_{SC} of 38.7 mA/cm^2 of this FTC-MWT-PERC device is significantly above the values achieved with a full area Al-BSF reference process confirming the feasibility of the novel rear contacting approach. Due to the early stage of FTC paste development, the contact resistance of the fire-through contacts is still non-optimal. Microstructure analysis revealed only partial alloying through the dielectric within the fire-through area as a main reason for the increased contact resistance. Future optimisation of the paste composition is expected to solve this issue.

Interesting possibilities to further decrease the recombination at the local contacts are the usage of additional FTC paste additives to improve local BSF formation and Al alloying. The possibility of such a separate optimisation of the paste surrounding the local contacts is a major advantage compared to other rear contacting methods such as LFC and i-PERC.

Acknowledgements

The Authors acknowledge the support of all co-workers at Fraunhofer ISE and the partial funding of this work by the German Federal Ministry for the Environment, Nature Conservation and Nuclear Safety (BMU) under contract no. 0329849B. The contribution of DEK solar is gratefully acknowledged.

References

[1] A.W. Blakers, A. Wang, A.M. Milne, J. Zhao, M.A. Green, 22.8% efficient silicon solar cell, Applied Physics Letters, 55 (1989) 1363-1365.
[2] G. Agostinelli, P. Choulat, H.F.W. Dekkers, S. De Wolf, G. Beaucarne, Screen printed large area crystalline silicon solar cells on thin substrates, in: Proceedings of the 20th European Photovoltaic Solar Energy Conference, Barcelona, Spain, 2005, pp. 647-650.
[3] R. Preu, S.W. Glunz, S. Steinbühl, W. Pfleging, W. Wettling, Laser ablation - A new low-cost approach for passivated rear contact formation in crystalline silicon solar cell technology, in: European Photovoltaic Solar Energy Conference, Glasgow, 2000.
[4] K.A. Münzer, J. Schöne, M. Hein, A. Teppe, R.E. Schlosser, M. Hanke, J. Maier, K. Varner, S. Keller, P. Fath, Development and implementation of 19% rear passivation and local contact centaurus technology, in: Proceedings of the 26th European Photovoltaic Solar Energy Conference and Exhibition, Hamburg, Germany, 2011, pp. 2292-2297.
[5] E. Schneiderlöchner, R. Preu, R. Lüdemann, S.W. Glunz, G. Willeke, Laser-fired contacts (LFC), in: Proceedings of the 17th European Photovoltaic Solar Energy Conference, WIP-Munich and ETA-Florence, Munich, Germany, 2001, pp. 1303-1306.
[6] A. Mohr, S. Wanka, A. Stekolnikov, M. Scherff, R. Seguin, P. Engelhart, C. Klenke, J.Y. Lee, S. Tardon, S. Diez, J. Wendt, B. Hintze, R. Hoyer, S. Schmidt, J.W. Müller, P. Wawer, Large area solar cells with efficiency exceeding 19% in pilot series designed for conventional module assembling, Energy Procedia, 8 (2011) 390-395.
[7] G. Schubert, B. Fischer, P. Fath, Formation and nature of Ag thick film front contacts on crystalline silicon solar cells, in: PV in Europe - From PV Technology to Energy Solutions, Rome, Italy, 2002, pp. 343-346.
[8] L. Janßen, M. Rinio, D. Borchert, H. Windgassen, D.L. Bätzner, H. Kurz, Thin bifacial multicrystalline silicon solar cells for industrial production, in: Proceedings of the 21st European Photovoltaic Solar Energy Conference, Dresden, Germany, 2006, pp. 834-837.
[9] C.-H. Du, S.-P. Hsu, Method of Manufacturing Back Electrode of Silicon Bulk Solar Cell, Pub. No. US 2010/0098840 A1, 2010.
[10] R.A. Sinton, A. Cuevas, Contactless determination of current-voltage characteristics and minority-carrier lifetimes in semiconductors from quasi-steady-state photoconductance data, Applied Physics Letters, 69 (1996) 2510-2512.
[11] J.-F. Nekarda, Laser Fired Contacts (LFC) - Charakterisierung, Optimierung und Modellierung eines Verfahrens zur lokalen Rückseitenkontaktierung dielektrisch passivierter Silizium-Solarzellen, in: Fakultät für Physik, Universität Konstanz, 2012.
[12] M.J. Kerr, A. Cuevas, General parameterization of Auger recombination in crystalline silicon, Journal of Applied Physics, 91 (2002) 2473-2480.
[13] D.A. Clugston, P.A. Basore, PC1D version 5: 32-bit solar cell modeling on personal computers, in: Proceedings of the 26th IEEE Photovoltaic Specialists Conference, IEEE; New York, NY, USA, Anaheim, California, USA, 1997, pp. 207-210.
[14] J. Nekarda, S. Stumpp, L. Gautero, M. Hörteis, A. Grohe, D. Biro, R. Preu, LFC on screen printed aluminium rear side metallization, in: Proceedings of the 24th European Photovoltaic Solar Energy Conference, Hamburg, Germany, 2009, pp. 1411-1415.
[15] A. Wolf, D. Biro, J.-F. Nekarda, S. Stumpp, A. Kimmerle, S. Mack, R. Preu, Comprehensive analytical model for locally contacted rear surface passivated solar cells, Journal of Applied Physics, 108 (2010) 1-13.
[16] B. Thaidigsmann, A. Drews, T. Fellmeth, P. Saint-Cast, A. Wolf, F. Clement, R. Preu, B. Biro, Synergistic effects of rear-surface passivation and the metal wrap through concept, IEEE Journal of Photovoltaics, 2 (2012) 109-113.